Electrochimica Acta 263 (2018) 53–59

Contents lists available at ScienceDirect

Electrochimica Acta

journal homepage: www.elsevier.com/locate/electacta

Highly crosslinked organosulfur copolymer nanosheets with abundant mesopores as cathode materials for efficient lithium-sulfur batteries

Shuaibo Zeng [a], Ligui Li [a, b, *], Jingping Yu [a], Nan Wang [a], Shaowei Chen [a, c, **]

[a] Guangzhou Key Laboratory for Surface Chemistry of Energy Materials, New Energy Research Institute, College of Environment and Energy, South China University of Technology, Guangzhou Higher Education Mega Center, Guangzhou 510006, China
[b] Guangdong Provincial Key Laboratory of Atmospheric Environment and Pollution Control, College of Environment and Energy, South China University of Technology, Guangzhou 510006, China
[c] Department of Chemistry and Biochemistry, University of California, 1156 High Street, Santa Cruz, CA 95064, USA

ARTICLE INFO

Article history:
Received 11 October 2017
Received in revised form
5 December 2017
Accepted 30 December 2017
Available online 3 January 2018

Keywords:
Lithium-sulfur battery
Cycling performance
Chemical confinement
Inverse vulcanization
Crosslinked copolymer

ABSTRACT

Low sulfur utilization and poor cycling stability are two major factors that currently impede the widespread commercialization of lithium-sulfur (Li-S) batteries. Herein, sulfur-rich side chains are anchored onto Schiff-base copolymer of thiourea aldehyde resin (cp (S-TAR)) nanosheets via inverse vulcanization to form a large number of intermolecular crosslinkers as well as mesopores. Application of the resultant copolymer as a cathode material in Li-S batteries can not only provide abundant porous channels for Li^+ diffusion but also significantly alleviate the dissolution of polysulfides by chemical confinement through the covalent bonds between sulfur-rich side chains and TAR. With this novel polymer cathode, a Li-S battery prototype is constructed which can operate at 1 C for over 500 charge-discharge cycles at nearly 99% coulombic efficiency, showing an ultralow cyclic fading rate of 0.045% per cycle, and an outstanding high-rate response of up to 5 C. The present strategy demonstrates the great potential of using highly crosslinked organosulfur copolymers as high-performance polymer cathode materials for low-cost, high-energy density Li-S batteries.

1. Introduction

Rechargeable lithium-sulfur (Li-S) batteries represent one of the most promissing next-generation energy storage technologies owing to various advantages, such as high theoretical energy density (2600 Wh/Kg), environmental inertness and natural abundance of sulfur in the earth crust as well as low operation costs [1–4]. However, the mass-scale application is impeded by a series of technical challenges, primarily from the cathode side: (i) low utilization of sulfur due to the intrinsic poor electronic conductivity of elementary sulfur, *ca.* 5×10^{-30} S/cm at 25 °C [5–7]; and (ii) rapid capacity decay resulting from the dissolution and migration of long-chain polysulfides (Li_2S_x ($x = 4$ to 8)) [8–10] as well as the delamination of active sulfur-containing materials from electrode because of their severe volume fluctuation during lithiation/delithiation processes [11–13]. To mitigate these scabrous issues, great efforts have been devoted to the design and preparation of various conductive frameworks to encapsulate sulfur-containing composites [14,15], such as graphene [16–19], conductive polymers [20–22], porous carbons [23–25], metal oxides [26,27] and other novel architectures [10,26,28]. Indeed, these conductive frameworks can provide a high surface area, effectively hold the sulfur particles and hence increase the conductivity of the sulfur cathodes, which not only substantially enhances the utilization of sulfur, but also alliviates the negative effects of polysulfide shuttling between the electrodes by physically restraining polysulfides within the porous textures of the conductive frameworks [29,30]. However, controlled synthesis of conductive frameworks with desired porous textures is difficult, and it usually involves multiple time- and energy-consuming processes, which is not beneficial to large-scale commercialization [31–33]. Moreover, severe dissolution of polysulfides still occurs in prolonged cycling due to the lack

* Corresponding author. Guangzhou Key Laboratory for Surface Chemistry of Energy Materials, New Energy Research Institute, College of Environment and Energy, South China University of Technology, Guangzhou Higher Education Mega Center, Guangzhou 510006, China.
** Corresponding author. Guangzhou Key Laboratory for Surface Chemistry of Energy Materials, New Energy Research Institute, College of Environment and Energy, South China University of Technology, Guangzhou Higher Education Mega Center, Guangzhou 510006, China.
E-mail addresses: esguili@scut.edu.cn (L. Li), shaowei@ucsc.edu (S. Chen).

https://doi.org/10.1016/j.electacta.2017.12.179
0013-4686/

of chemical confinement of polysulfides. Therefore, concurrent introduction of both physical and chemical confinements to polysulfides is highly desired to effectively mitigate the dissolution of polysulfides and hence increase the cycling stability of battery.

Recently, utilizing polymers consisting of a high content of organosulfur that is homogeneously distributed and covalently bonded to polymer backbones [34–36] has been reported to be a noteworthy strategy to endow both physical and chemical confinements on the soluble polysulfide [34,37,38] intermediates Li_2S_x ($4 \leq x \leq 8$) in liquid electrolyte which are generated during discharge process through the overall reaction: $16Li + S_8 \rightarrow 8Li_2S$ [39,40]. Yet, it remains difficult to synthesize organosulfur copolymer nanosheets with mesopores that include abundant Li^+ diffusion channels [41,42] so that high charge/discharge rate can be achieved [43,44].

Herein, sulfur-containing copolymer nanosheets comprising a large number of mesoporous textures are prepared by sulfurization of TAR and used as cathode materials for Li-S batteries to impede the formation of soluble high-order Li_2S_n ($4 \leq n \leq 8$). The resulting novel cp (S-TAR) cathode consists of abundant hyper-branched organosulfur networks, which leads to excellent cycling stability, with an ultralow fading rate of only 0.045% per cycle and a coulombic efficiency of 99% due to formation of cross-linkings between sulfur and TAR. Moreover, the mesoporous cp (S-TAR) nanosheets also provides abundant Li^+ diffusion channels, which effectively improves the utilization of sulfur ad rate performance. These morphology advantages contribute to a high initial capacity of 1285 mAh g^{-1} as well as excellent rate capacity of 1176 mAh g^{-1} at 0.2 C, 852 mAh g^{-1} at 1 C and 535 mAh g^{-1} at 5 C.

2. Experimental section

Synthesis of TAR: 6 g of thiourea was dissolved in DI-water (150 mL) under magnetic stirring in an Ar-filled round-bottom flask. The temperature of the solution was maintained at 50 °C with a water bath. Subsequently, 8 mL of a formaldehyde solution (38 wt %) and 0.5 mL of a hydrochloric acid aqueous solution (37 wt%) was added slowly into the above solution under magnetic stirring. The color of the mixture gradually changed from colorless to milky white, signifying the formation of TAR. The reaction was allowed to proceed for 3 h. Finally, the solid product was collected and washed with DI-water for several times, and dried at 30 °C in a vacuum oven, affording the dried TAR product.

Preparation of cp(S-TAR): The TAR obtained above was mixed with sulfur at a mass ratio of TAR: sulfur (S_8) of 1:7. The mixtures were heated at 140 °C for 1 h to impregnate the molten sulfur into TAR in an Ar atmosphere, and then at 170 °C for 8 h to initiate the ring-opening polymerization of sulfur with TAR, leading to the formation of highly crosslinked cp (S-TAR) copolymer. The overall synthetic strategy of cp (S-ATR) is schematically illustrated in Fig. 1a.

Materials Characterization: Scanning electron microscopy (SEM) measurements were performed with a Hitachi S-4800 field emission scanning electron microscopy (FESEM). Transmission electron microscopy (TEM) measurements were conducted on a JEOL JEM-2100 transmission electron microscopy with an accelerating voltage of 200 kV. FTIR spectra were recorded on a Nicolet 6700 FTIR spectrometer in a transmittance mode. UV–Vis absorption measurements were carried out with a UV-2600 spectrophotometer. Nitrogen adsorption-desorption isotherm measurements were performed on a Quadrasorb instrument. X-ray photoelectron spectroscopy (XPS) measurements were conducted on a Phi X-tool XPS instrument. Differential scanning calorimetry (DSC) analysis was conducted on a METTLER instrument under a N_2 atmosphere at a ramping rate of 10 °C min^{-1}. For electrical conductivity measurements, the powder materials were compressed at a pressure of 40 MPa to form circular sheets with the same diameter using a tablet compression machine. The electrical conductivity was measured on a KEITHLEY 2636B source-meter using a two-probe method.

Coin-cell fabrication and battery tests: polyvinylidene fluoride (PVDF) binder was dissolved completely in N-methyl-2-pyrrolidene (NMP) under vigorous magnetic stirring for 20 min. The active material of cp (S-TAR) and conductive carbon black were added into the PVDF solution to form a homogenous slurry at a mass ratio of 70:20:10 for cp (S-TAR):PVDF:conductive carbon black. Subsequently, the slurry was deposited on an Al foil that was used as a current collector by a doctor blade method and then dried at 45 °C for 24 h in a vacuum oven to form a thin film with a thickness of ca. 250 μm. The thus-prepared cathode foil was compressed to obtain a thickness of 80 μm and then cut into circular sheets of 12 mm in diameter as reported by Woo Jin Chung et al. [42] and Bernd Oschmann et al. [43] The loading of active sulfur was calculated to be 1.6 mg cm^{-2}. The CR2032-type coin cells were assembled in an Ar-filled glove box with both oxygen and moisture contents lower than 0.1 ppm. The cell comprised a cathode of cp (S-TRA), a diaphragm Celgard 2400 separator, a reference/counter electrode of a lithium foil, and the mixed solution of 1,3-dioxolane and 1,2-dimethoxyethane (1:1, v/v) containing 1 M lithium bis(-trifluromethanesulfonyl) imide (LiTFSI) and 0.1 M $LiNO_3$ as the electrolyte. For comparison, coin cells with the simple mixture of TAR and S as the cathode materials (denoted as S + TAR) were prepared in a similar manner at the same loading of active sulfur. In addition, conventional sulfur cathodes were also prepared according to the same procedures at a mass ratio of sulfur:conductive carbon black:PVDF = 50:40:10, again, at the same mass loading of active sulfur.

Galvanostatic discharge-charge measurements of the as-fabricated cells were performed by potential cycling between 1.5 and 3.0 V (vs. Li/Li^+) at different current rates using a button cell testing system (LANHE CT2001A 5 V 20 mA). Cyclic voltammograms (CV) were acquired within the potential range of 1.5–3.0 V at varied scan rates. Electrochemical impedance spectroscopy (EIS) studies were carried out in charged state between the frequency of 100 kHz and 10 MHz at an AC amplitude of 5 mV.

3. Results and discussion

3.1. Mechanism

The correlated charge-discharge reactions for cathode in Li-S battery are shown in Fig. S1. During the charge process, the first peak at 2.20 V is associated with the formation of low-order Li_2S_n, which is oxidized further to the high-order Li_2S_n ($6 \leq n \leq 8$) and S_8 at 2.50 V (Fig. S1) [39]. The oxidation peak at 2.50 V disappears in the CV curves for cp (S-TAR) cathodes, which signifies the formation of cross-linking between sulfur and TAR instead of isolated high-order Li_2S_n ($6 \leq n \leq 8$) and S_8.

3.2. Morphology and structural analysis

The production of cp (S-TAR) with abundant sulfur side chains as intermolecular crosslinkers may effectively prevent the dissolution of polysulfide compounds in the cathodes of Li-S batteries by chemical confinement of the covalent bonds between sulfur side chains and TAR backbones (Fig. 1b). From the SEM measurements depicted in Fig. 2a and b, one can see that the as-prepared TAR consists of a large number of thin nanosheets with a thickness of tens of nanometers and a lateral size of several microns. After copolymerization with sulfur, the TAR nanosheet surface becomes

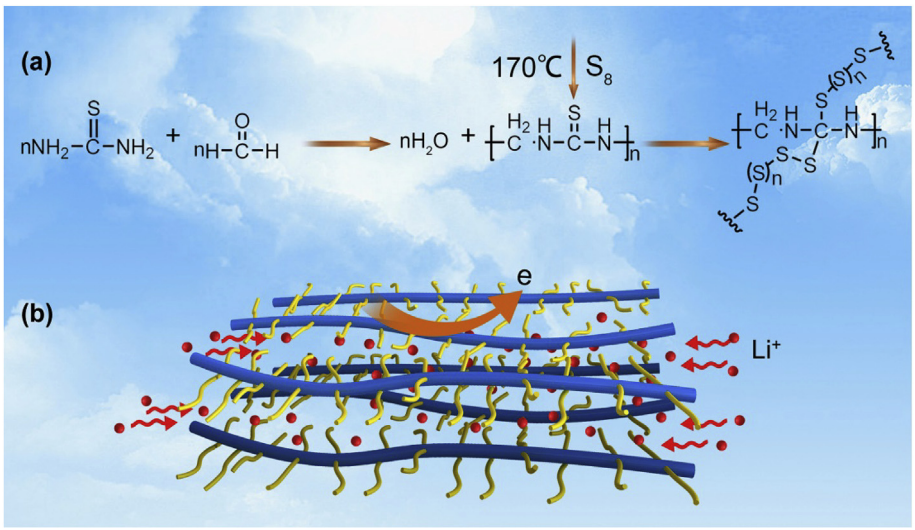

Fig. 1. (a) Synthetic procedure of cp (S-TAR). (b) Schematic illustration of the chemical sturcture of cp (S-TAR).

roughened, decorated with a large number of pores with diameters ranging from tens of nanometers to hundreds of nanometers (Fig. 2c and d), while coexistence of irregular sulfur nanoparticles and non-porous TAR nanosheets is observed for the blend sample S + TAR (Fig. S2). From the corresponding TEM image in Fig. 2e, one can find that cp (S-TAR) largely maintains the sheet-like morphology but consists of abundant porous structures. Fig. 2f depicts a higher-magnification TEM image, from which the pore size in the sheet-like cp (S-TAR) can be estimated to be 6.20 ± 1.56 nm. Fig. 2g shows the N_2 adsorption/desorption isotherms of cp (S-TAR), where the BET specific surface area and Barrett-Joyner Halenda (BJH) pore volume can be calculated from the N_2 desorption isotherm to be 8.93 $m^2 g^{-1}$ and 0.028 $cm^3 g^{-1}$, respectively. The corresponding pore-size distribution plot (inset to Fig. 2g) reveals the formation of mesopores in cp (S-TAR) with a pore size ranging from 1.30 nm to 7.00 nm, in good agreement with

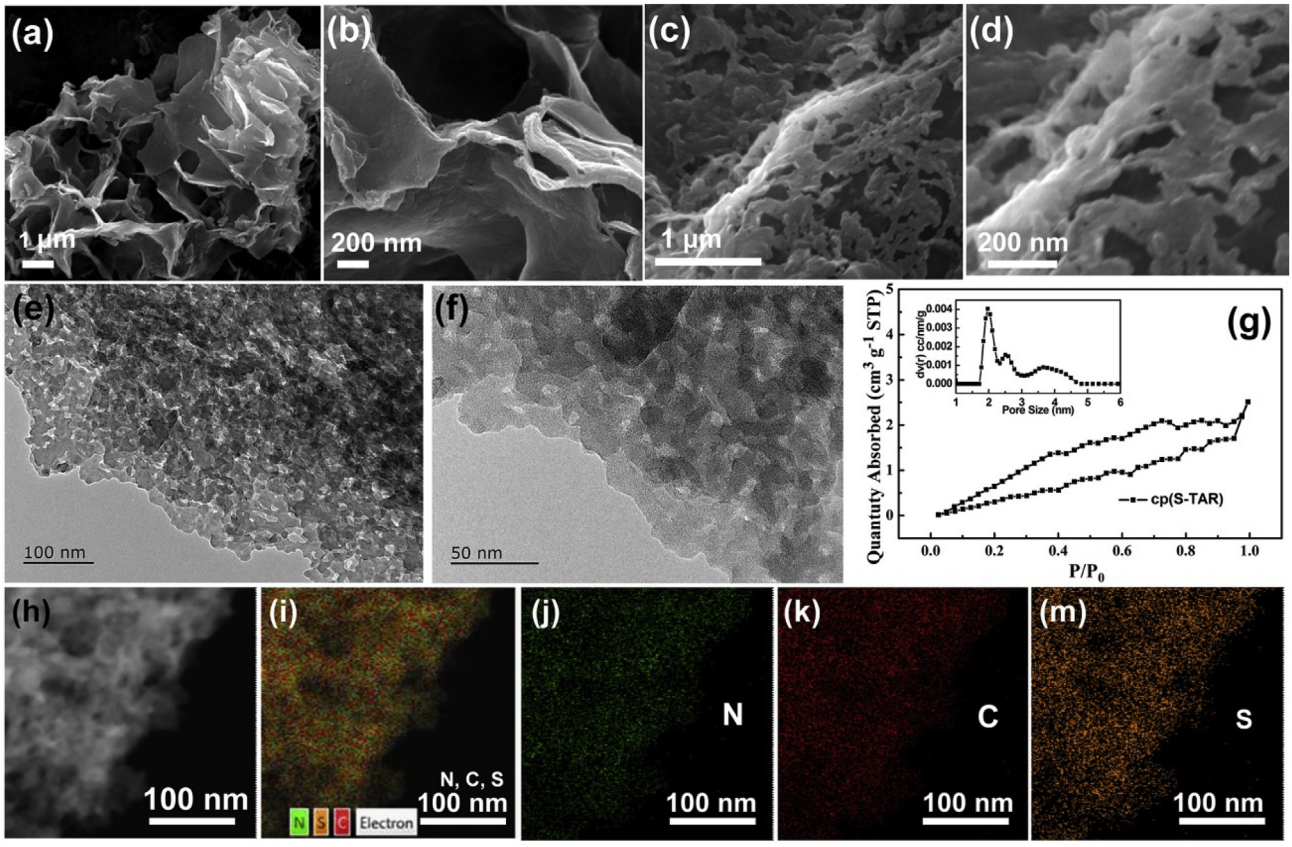

Fig. 2. SEM images of (a, b) TAR; (c, d) cp (S-TAR). (e, f) TEM image of cp (S-TAR). (g) N_2 adsorption/desorption isotherms of cp (S-TAR). Inset is the corresponding pore-size distribution plot. (h) TEM image showing the morphology of selected area of cp (S-TAR) and the corresponding elemental maps of (i) N, C, S; (j) N; (k) C and (m) S.

the TEM results in Fig. 2e and f. Furthermore, elemental mapping analysis of a selected area (Fig. 2h) shows that S, N and C elements are distributed uniformly throughout the entire sample (Fig. 2i–m). These structural merits enable a quick diffusion of lithium ions into the interior of cp (S-TAR) and also maximize the exposure of cp (S-TAR) to electrolyte to realize better utilization of loaded sulfur. From the EDS spectrum in Fig. 3a, the concentration is determined to be 16.05 wt% for C, 5.62 wt% for N, 3.33 wt% for O and 75.00 wt% for S. For the DSC curves depicted in Fig. 3b, four pronounced peaks are observed, where the first one at about 107 °C is attributed to the solid-to-solid conversion of sulfur from the orthorhombic phase to monoclinic phase, the second one at about 120.0 °C is due to melting, the third one at about 170.0 °C is ascribed to the breakage of the S–S bond in S_8 to form diaradicals, while the fourth one at about 315 °C is much broader than the other three and is probably due to the boiling of liquid sulfur. By comparison of the DSC curve of cp (S-TAR) with that of pure sulfur, one can find that the endothermal peak at about 170 °C is significantly reduced (dashed circle), indicating that the elementary sulfur is partially covalently bonded to TAR to form crosslinked cp (S-TAR). Besides, the formation of crosslinked cp (S-TAR) is evidenced by the color change from light yellow for the mixture of sulfur and TAR to taupe for the final product (Fig. S3). The formation of crosslinked cp (S-TAR) can be further supported by the results of XPS measurements. From the survey spectrum (Fig. S4), a series of peaks can be identified at about 285.0 eV for C 1s, 226.0 eV for S 2s, 164.0 eV for S 2p, 532.0 eV for N 1s and 398.0 eV for O 1s electrons. Fig. 3c depicts the high resolution spectrum of the C 1s electrons, which can be deconvoluted into four subpeaks at 284.4 eV, 285.7 eV, 287.2 eV and 288.7 eV, due to C–C/C=C, C–N/C–S, C=O and O–C=O, respectively [45,46]. The presence of C–S groups in cp (S-TAR) signifies that C=S groups on sulfourea can largely persist during the multi-step synthesis process. For the corresponding high-resolution S 2p spectrum, deconvolution of the original plot yields three peaks at 163.9 eV, 165.0 eV and 168.8 eV (Fig. 3d), corresponding to S $2p_{1/2}$, S $2p_{3/2}$ and S-C, respectively [47–49]. The formation of S–C groups also confirms that S=C groups in sulfourea is preserved during the synthesis of TAR and subsequently forms crosslinked structures via vulcanization. In order to quantitatively determine the content of sulfur in cp (S-TAR) that is covalently crosslinked with the C=S groups, cp (S-TAR) is dispersed into CS_2 to dissolve the non-crosslinked sulfur. UV–vis absorption measurements show that about 51.0 wt% of the total sulfur is covalently bonded with TAR (Fig. S5).

3.3. Electrochemical performance

The performance of cp (S-TAR) cathode is then evaluated by CV measurements. As depicted in Fig. 4a, two clear reduction peaks emerge when the potential is scanned negatively from +3.0 V to +1.5 V (vs. Li^+/Li), where the one at about 2.25 V is due to the formation of high-order Li_2S_n ($6 < n < 8$) species and hence corresponds to the first discharge platform in the discharge curve (Fig. 4b), while the other one located at about 2.04 V is ascribed to the further reduction of relatively long-chain polysulfudes to short-chain Li_2Sn ($n < 4$) and finally Li_2S, which constitutes the second discharge platform in Fig. 4b [40]. In the positive potential scan, only one peak at about +2.5 V (vs. Li^+/Li) is observed due to the oxidation of Li_2S to polysulfides. It is worthy to note that the oxidation peak position gradually shifts to a lower potential when the number of discharge-charge cycling increases from 1 to 20, which indicates that a lower charge-discharge potential gap is obtained for the cp (S-TAR) based cathode in this "activation" process. From the typical discharge curves for S/C, S + TAR/C and cp (S-TAR)/C electrodes showed in Fig. 4b, one can find that all electrodes show two typical platforms, coinciding with the two-stage reduction process of sulfur during discharging [39,40,50]. In the charge process, all electrodes show a platform at around +2.3 V that is ascribed to the aforementioned transformation of short-chain polysulfides to longer-chain polysulfides. However, an

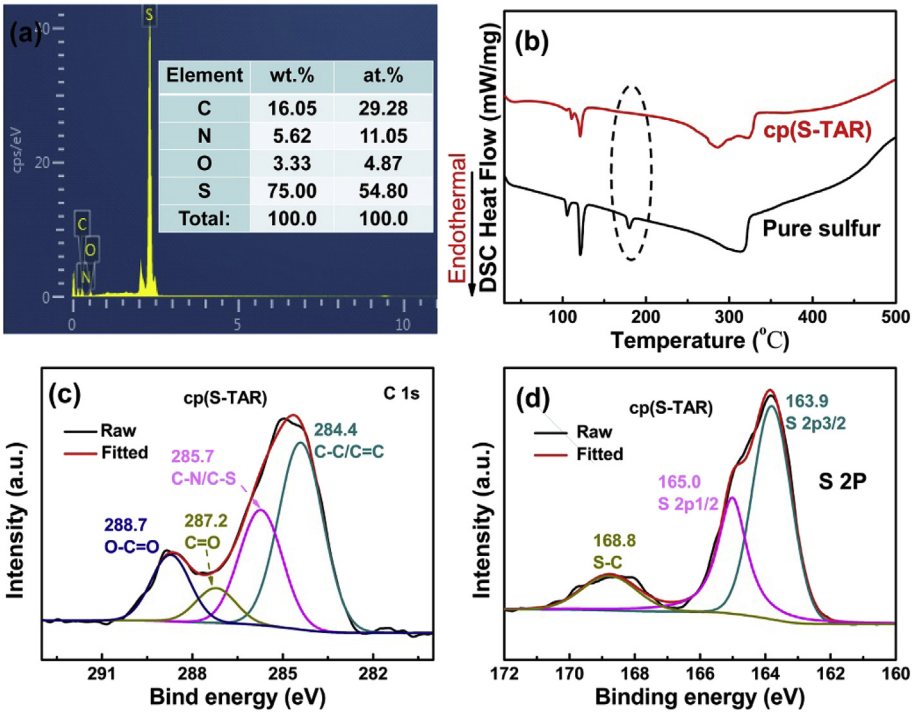

Fig. 3. (a) EDS spectrum of cp (S-TAR); inset is a table summarizing the contents of different elements in the sample. (b) DSC curves of pure sulfur and cp (S-TAR). High-resolution XPS spectra of (c) C 1s and (d) S 2p electrons in cp (S-TAR). Black curves are experimental data and colored curves are deconvolution fits.

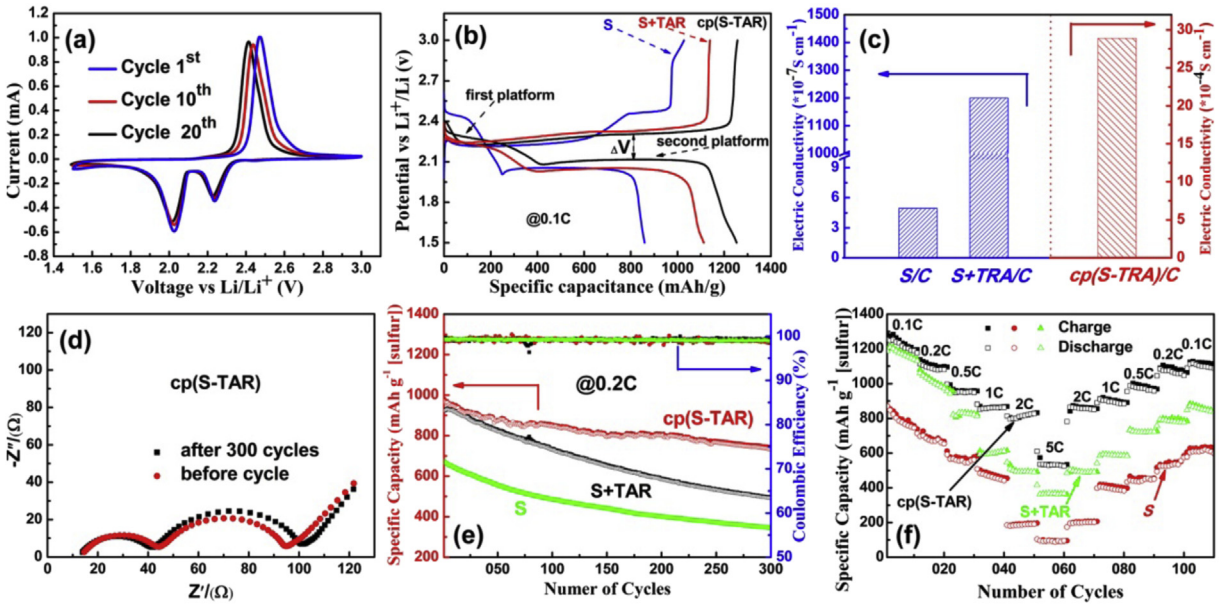

Fig. 4. (a) CV curves for a coin-type Li-S battery with a cp (S-TAR)-based cathode. (b) Typical charge and discharge curves for Li-S batteries with S/C, S + TAR/C and cp (S-TAR)/C electrodes at 0.1 C. (c) Electrical conductivity of S/C, S + TAR/C and cp (S-TAR)/C electrodes. (d) EIS curves of cp (S-TAR)-based cathode before and after 300 discharge-charge cycles. (e) Cycling performance and coulombic efficiency of S, S + TAR and cp (S-TAR) based electrodes at 0.2 C. (f) Rate capacity of the S, S + TAR and cp (S-TAR) based electrodes at varied rates.

additional platform is observed at +2.475 V (vs. Li^+/Li) for the S/C electrode due to the transformation of long-chain polysulfides to S_8. The disappearance of the additional platform at +2.475 V (vs. Li^+/Li) for S + TAR/C and cp (S-TAR)/C electrodes signifies that sulfur in these two samples is more effectively confined to prevent the formation of S_8, where sulfur in S + TAR sample may react with TAR during charging. Significantly, the cp (S-TAR)/C electrode delivers a much higher reversible discharge-charge capacity of 1285 mAh g^{-1} at 0.1 C, as compared with the 850 mAh g^{-1} for S/C and 1105 mAh g^{-1} for S + TAR/C electrodes. Additionally, one can find that the potential gap between the charge and discharge curves for cp (S-TAR) is much smaller than that for S/C and S + TAR/C electrodes. These results signify a remarkably improved electrochemical kinetics upon copolymerization of sulfur and TAP in cp (S-TAR).

Electrical conductivity measurments reveal that the conductivity is increased by nearly 3 orders of magnitude from 4.5×10^{-7} S cm^{-1} for S/C to 1.2×10^{-4} S cm^{-1} for S + TAR/C and 2.8×10^{-3} S cm^{-1} for cp (S-TAR)/C (Fig. 4c), which is likely attributed to the improved contact between sulfur and TAR resulting from the covalent bonds between them. It shows that the high electrical conductivity of cp (S-TAR)/C electrode is preserved during long-term discharge-charge cycling. As exhibited in Fig. 4d, the electrical resistance is largely unchanged after 300 cycles, with a low resistance of *ca.* 115Ω.

Fig. 4e depicts the cycling performances of different electrodes at a sulfur loading of 1.6 mg cm^{-2} at 0.2 C. It is found that although the three samples show a comparable coulombic efficiency, the cp (S-TAR)/C electrode delivers the highest initial capacitance of 969 mAh g^{-1}, as compared with the 667 mAh g^{-1} for S/C and 921 mAh g^{-1} for S + TAR/C. After 300 cycles, the cp (S-TAR)/C electrode still shows a retention capacity of 732 mAh g^{-1}, which is much higher than those for S/C (341 mAh g^{-1}) and S + TAR/C (493 mAh g^{-1}). The rate performance of the three electrodes are evaluated by galvanostatic charge-discharge at various current rates. As shown in Fig. 4f and S6, the cp (S-TAR)/C electrode exhibits excellent rate performance, for example, with an extremely high specific discharge capacity of 1285 mAh g^{-1} at 0.1 C, 1176 mAh g^{-1} at 0.2 C, 959 mAh g^{-1} at 0.5 C, 852 mAh g^{-1} at 1 C, 794 mAh g^{-1} at 2 C, and 535 mAh g^{-1} at 5 C. After 100 cycles, the specific capacity is recovered to 1089 mAh g^{-1} at 0.1 C. All these values are much higher than those for S/C and S + TAR/C electrodes. These values of present work are better than or at least comparable to those based on different methods reported in recent literature (Table S1). The remarkable performance was attributed to the synergetic effects of following factors: (1) sulfur is successfully anchored onto polymer backbones and form mesoporous structures, which help increase the electrical conductivity and utilization of sulfur. (2) the dissolution and diffusion of polysulfides is effectively supressed by the coexistence of physical and chemical confinement resulting from the high density of chemical bonds between sulfur and TAR. During discharge, sulfur side chains in cp (S-TAR) may react with Li^+ to form Li-S_n-TAR that is covalently bonded with TAR, hence restraining the dissolution of sulfur in cp (S-TAR). (3) The mesoporous cp (S-TAR) nanosheets also afford abundant short Li^+ diffusion channels.

3.4. Stability of cathode

The long-term cycling stability for different cathode materials is investigated at a current density of 1 C. As shown in Fig. 5 and S7, the cp (S-TAR)/C electrode delivers a high capacity of 819 mA h/g after 500 cycles, with an ultralow cyclic fading rate of only 0.045% per cycle while the capacity of S/C electrode rapidly diminishes to about 310 mA h/g after just 200 cycles, at a much higher fading rate of 0.237% per cycle. The high stability of cp (S-TAR)/C electrode is attributed to chemical restraint of polysulfides by the crosslinked structures between sulfur and TAR backbones.

The morphology of the electrodes before and after 500 discharge-charge cycles at 1C is then examined by SEM measurements. As depicted in Fig. S8, the morphology of the S/C and cp (S-TAR)/C electrodes before cycling looks similar, with dense nanoparticles distributing on the surface. After 500 cycles, a large number of micron-sized holes/pores appear on the surface of the S/C electrode due to the dissolution of polysulfides from the electrode

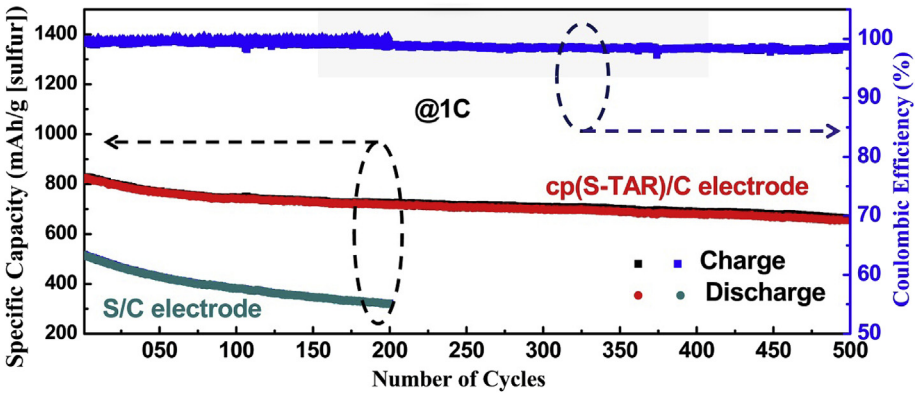

Fig. 5. (a) Long-term cycling performance and coulombic efficiency for cp (S-TAR)/C and S/C at 1 C.

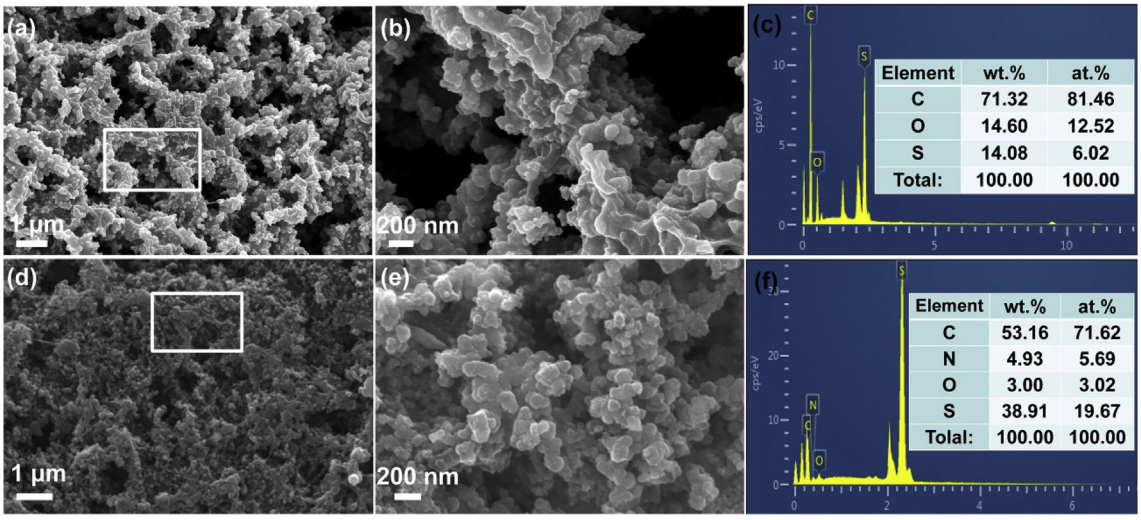

Fig. 6. (a, b) SEM images and (c) EDS spectrum of the S/C electrode after 500 discharge-charge cycles at 1 C; inset to panel (c) is the summary of the elemental contents. (d, e) SEM images and (f) EDS spectrum of cp (S-TAR)/C electrode after 500 discharge-charge cycles at 1C; inset is the summary of the elemental contents.

into electrolyte (Fig. 6a and b). Correspondingly, the content of sulfur in S/C electrode drastically decreased from the initial 50.2 wt % to only 14.1 wt%, as manifested by EDS measurements (Fig. 6c). In sharp contrast, the cp (S-TAR)/C electrode largely retains its initial morphology after 500 cycles (Fig. 6d–e), and the corresponding EDS measurements show that a much higher sulfur content of 38.91 wt% is retained in cp (S-TAR), i.e., 43.17% of the sulfur in the original cp (S-TAR) survives after 500 discharge-charge cycles. These observations clearly demonstrate that crosslinking sulfur with TAR via covalent bonds significantly restrains the dissolution of polysulfides and hence enhances the cycling stability of cp (S-TAR) based cathodes in Li-S batteries.

4. Conclusion

In summary, cp (S-TAR) nanosheets were synthesized by direct vulcanization of TAR where more than half of the feeding sulfur formed highly crosslinked structures with the TAR backbones. The resulting cp (S-TAR) comprised abundant mesopores, which not only provided short channels for efficient Li^+ diffusion, hence leading to high utilization of sulfur and showing a high initial capacity of 1285 mAh g^{-1}, but also remarkably increased the rate performance, with 1176 mAh g^{-1} at 0.2 C, 959 mAh g^{-1} at 0.5 C, 852 mAh g^{-1} at 1 C, 794 mAh g^{-1} at 2 C, and 535 mAh g^{-1} at 5 C. Moreover, the formation of covalent bonds between suflur and TAR significantly increased the cycling stability of the cathodes in Li-S batteries, at an ultralow fading rate of only 0.045% per cycle during the 500 discharge-charge cycles.

Acknowledgements

This work was supported by the National Natural Science Foundation of China (NSFC 21528301 and 51402111), Guangdong Innovative and Entrepreneurial Research Team Program (2014ZT05N200), and the Fundamental Research Funds for the Central Universities (SCUT Grant No. 2153860).

Appendix A. Supplementary data

Supplementary data related to this article can be found at https://doi.org/10.1016/j.electacta.2017.12.179.

References

[1] L. Borchardt, M. Oschatz, S. Kaskel, Carbon materials for lithium sulfur batteries-ten critical questions, Chem. Eur J. 22 (22) (2016) 7324–7351.
[2] V. Etacheri, R. Marom, R. Elazari, G. Salitra, D. Aurbach, Challenges in the development of advanced Li-ion batteries: a review, Energy Environ. Sci. 4 (4) (2011) 3243–3262.
[3] N. Osada, C.B. Bucur, H. Aso, J. Muldoon, The design of nanostructured sulfur

cathodes using layer by layer assembly, Energy Environ. Sci. 9 (5) (2016) 1668–1673.
[4] Y. Xiang, J. Li, J. Lei, D. Liu, Z. Xie, D. Qu, et al., Advanced separators for lithium-ion and lithium-sulfur batteries: a review of recent progress, ChemSusChem 9 (2016) 3023–3039.
[5] F. Wu, J. Qian, R. Chen, T. Zhao, R. Xu, Y. Ye, et al., Sulfur cathode based on layered carbon matrix for high-performance Li-S batteries, Nano Energy 12 (2015) 742–749.
[6] C. Wu, L. Fu, J. Maier, Y. Yu, Free-standing graphene-based porous carbon films with three-dimensional hierarchical architecture for advanced flexible Li-sulfur batteries, J. Mater. Chem. 3 (18) (2015) 9438–9445.
[7] L. Wang, Y. Zhao, M.L. Thomas, H.R. Byon, In situ synthesis of bipyramidal sulfur with 3D carbon nanotube framework for lithium-sulfur batteries, Adv. Funct. Mater. 24 (15) (2014) 2248–2252.
[8] L. Wang, D. Wang, F. Zhang, J. Jin, Interface chemistry guided long-cycle-life Li-S battery, Nano Lett. 13 (9) (2013) 4206–4211.
[9] J. Wang, J. Yang, C. Wan, K. Du, J. Xie, N. Xu, Sulfur composite cathode materials for rechargeable lithium batteries, Adv. Funct. Mater. 13 (6) (2003) 487–492.
[10] H. Wang, W. Zhang, H. Liu, Z. Guo, A strategy for configuration of an integrated flexible sulfur cathode for high-performance lithium-sulfur batteries, Angew. Chem. Int. Ed. 55 (12) (2016) 3992–3996.
[11] S. Li, T. Mou, G. Ren, J. Warzywoda, B. Wang, Z. Fan, Confining sulfur species in cathodes of lithium-sulfur batteries: insight into nonpolar and polar matrix surfaces, ACS Energy Lett 1 (2) (2016) 481–489.
[12] M. Li, Y. Zhang, X. Wang, W. Ahn, G. Jiang, K. Feng, et al., Gas pickering emulsion templated hollow carbon for high rate performance lithium sulfur batteries, Adv. Funct. Mater. 26 (2016) 8408–8417.
[13] H. Li, X. Yang, X. M Wang, M. Liu, F. Ye, J. Wang, et al., Dense integration of graphene and sulfur through the soft approach for compact lithium/sulfur battery cathode, Nano Energy 12 (2015) 468–475.
[14] M.S. Kim, J. Jeong, W.I. Cho, W. Kim, Synthesis of graphitic ordered mesoporous carbon with cubic symmetry and its application in lithium-sulfur batteries, Nanotechnology 27 (12) (2016), 125401.
[15] J. Kim, D.J. Lee, H.G. Jung, Y.K. Sun, J. Hassoun, B. Scrosati, An advanced lithium-sulfur battery, Adv. Funct. Mater. 23 (8) (2013) 1076–1080.
[16] N. Jung, S. Kwon, Dongwook Lee, D.M. Yoon, Y.M. Park, A. Benayad, et al., Synthesis of chemically bonded graphene/carbon nanotube composites and their application in large volumetric capacitance supercapacitors, Adv. Mater. 25 (47) (2013) 6854–6858.
[17] S. Mondal, U. Rana, S. Malik, Graphene quantum dot-doped polyaniline nanofiber as high performance supercapacitor electrode materials, Chem. Commun. 51 (62) (2015) 12365–12368.
[18] J.L. Shi, C. Tang, H.J. Peng, L. Zhu, X.B. Cheng, J.Q. Huang, et al., 3D mesoporous graphene: CVD self-assembly on porous oxide templates and applications in high-stable Li-S batteries, Small 11 (39) (2015) 5243–5252.
[19] L. Ji, M. Rao, H. Zheng, L. Zhang, Y. Li, W. Duan, et al., Graphene oxide as a sulfur immobilizer in high performance lithium/sulfur cells, J. Am. Chem. Soc. 133 (46) (2011) 18522–18525.
[20] F.S. Li, Y.S. Wu, J. Chou, M. Winter, N.L. Wu, A mechanically robust and highly ion-conductive polymer-blend coating for high-power and long-life lithium-ion battery anodes, Adv. Mater. 27 (1) (2015) 130–137.
[21] L. Xiao, Y. Cao, J. Xiao, B. Schwenzer, M.H. Engelhard, L.V. Saraf, et al., A soft approach to encapsulate sulfur: polyaniline nanotubes for lithium-sulfur batteries with long cycle life, Adv. Mater. 24 (9) (2012) 1176–1181.
[22] C. Hong, W. Shengping, Recent progress in polymer/sulphur composites as cathodes for rechargeable lithium–sulphur batteries, J. Mater. Chem. 2 (34) (2014) 13783–13794.
[23] J. Schuster, G. He, B. Mandlmeier, T. Yim, K.T. Lee, T. Bein, et al., Spherical ordered mesoporous carbon nanoparticles with high porosity for lithium–sulfur batteries, Angew. Chem. Int. Ed. 51 (15) (2012) 3591–3595.
[24] Z.W. Seh, Y. Sun, Q. Zhang, Y. Cui, Designing high-energy lithium-sulfur batteries, Chem. Soc. Rev. 45 (2016) 5605–5634.
[25] J. Zhang, J. Xiang, Z. Dong, Y. Liu, Y. Wu, C. Xu, et al., Biomass derived activated carbon with 3D connected architecture for rechargeable lithium– sulfur batteries, Electrochim. Acta 116 (2014) 146–151.
[26] Z.W. Seh, W. Li, J.J. Cha, G. Zheng, Y. Yang, M.T. McDowell, et al., Sulphur–TiO_2 yolk–shell nanoarchitecture with internal void space for long-cycle lithium–sulphur batteries, Nat. Commun. 4 (2013) 1331–1336.
[27] M. Yan, Y. Zhang, Y. Li, Y. Huo, Y. Yu, C. Wang, et al., Manganese dioxide nanosheet functionalized sulfur@PEDOT core-shell nanospheres for advanced lithium-sulfur batteries, J. Mater. Chem. 4 (2016) 9403–9412.
[28] G. Zhou, S. Pei, L. Li, D.W. Wang, S. Wang, K. Huang, et al., A graphene-pure-sulfur sandwich structure for ultrafast, long-life lithium-sulfur batteries, Adv. Mater. 26 (4) (2014) 625–631.
[29] D. Bresser, S. Passerini, B. Scrosati, Recent progress and remaining challenges in sulfur-based lithium secondary batteries a review, Chem. Commun. 49 (49) (2013) 10545–10562.
[30] N. Deng, W. Kang, Y. Liu, J. Ju, D. Wu, L. Li, et al., A review on separators for lithiumsulfur battery: progress and prospects, J. Power Sources 331 (2016) 132–155.
[31] S. Diez, A. Hoefling, P. Theato, W. Pauer, Mechanical and electrical properties of sulfur-containing polymeric materials prepared via inverse vulcanization, Polymers 9 (2) (2017) 59–66.
[32] Z.A. Ghazi, L. Zhu, H. Wang, A. Naeem, A.M. Khattak, B. Liang, et al., Efficient polysulfide chemisorption in covalent organic frameworks for high-performance lithium-sulfur batteries, Adv. Eng. Mater. 6 (2016), 1601250.
[33] Y.X. Yin, S. Xin, Y.G. Guo, L.J. Wan, Lithium-sulfur batteries: electrochemistry, materials, and prospects, Angew. Chem. Int. Ed. 52 (50) (2013) 13186–13200.
[34] I. Gomez, D. Mecerreyes, J.A. Blazquez, O. Leonet, H.B. Youcef, C. Li, et al., Inverse vulcanization of sulfur with divinylbenzene: stable and easy processable cathode material for lithium-sulfur batteries, J. Power Sources 329 (2016) 72–78.
[35] H. Kim, Joungphil Lee, H. Ahn, O. Kim, M.J. Park, Synthesis of three-dimensionally interconnected sulfur-rich polymers for cathode materials of high-rate lithium-sulfur batteries, Nat. Commun. 6 (2015), https://doi.org/10.1038/ncomms8278.
[36] S. Zeng, L. Li, D. Zhao, J. Liu, W. Niu, N. Wang, et al., Polymer-capped sulfur copolymers as lithium-sulfur battery cathode: enhanced performance by combined contributions of physical and chemical confinements, J. Phys. Chem. C 121 (121) (2017) 2495–2503.
[37] N. Xu, T. Qian, X. Liu, J. Liu, Y. Chen, C. Yan, Greatly suppressed shuttle effect for improved lithium sulfur battery performance through short chain intermediates, Nano Lett. 17 (2017) 538–543.
[38] S. Zeng, L. Li, L. Xie, D. Zhao, N. Zhou, N. Wang, et al., Graphene-supported highly crosslinked organosulfur nanoparticles as cathode materials for high-rate, long-life lithium-sulfur battery, Carbon 122 (2017) 106–113.
[39] M.A. Pope, I.A. Aksay, Structural design of cathodes for Li-S batteries, Adv. Eng. Mater. 5 (2015), 1500124, https://doi.org/10.1002/aenm.201500124.
[40] Y. Li, J. Fan, M. Zheng, Q. Dong, A novel synergistic composite with multi-functional effects for high-performance Li-S batteries, Energy Environ. Sci. 9 (9) (2016) 1998–2004.
[41] H. Cheng, S. Wang, Recent progress in polymer/sulphur composites as cathodes for rechargeable lithium-sulphur batteries, J. Mater. Chem. 2 (34) (2014) 13783–13794.
[42] H. Hu, H. Cheng, Z. Liu, G. Li, Q. Zhu, Y. Yu, Situ polymerized PAN-Assisted S/C nanosphere with enhanced high-power performance as cathode for lithium/sulfur batteries, Nano Lett. 15 (8) (2015) 5116–5123.
[43] B. Oschmann, J. Park, C. Kim, K. Char, Y.E. Sung, R. Zentel, Copolymerization of polythiophene and sulfur to improve the electrochemical performance in lithium–sulfur batteries, Chem. Mater. 27 (20) (2015) 7011–7017.
[44] W.J. Chung, J.J. Griebel, E.T. Kim, H. Yoon, A.G. Simmon, H.J. Ji, et al., The use of elemental sulfur as an alternative feedstock for polymeric materials, Nat. Chem. 5 (6) (2013) 518–524.
[45] G. Li, J. Sun, W. Hou, S. Jiang, Y. Huang, J. Geng, Three-dimensional porous carbon composites containing high sulfur nanoparticle content for high-performance lithium-sulfur batteries, Nat. Commun. 7 (2016), 10601, https://doi.org/10.1038/ncomms10601.
[46] B. Li, S. Li, J. Xu, S. Yang, A new configured lithiated silicon–sulfur battery built on 3D graphene with superior electrochemical performances, Energy Environ. Sci. 9 (6) (2016) 2025–2030.
[47] K. Mi, Y. Jiang, J. Feng, Y. Qian, S. Xiong, Hierarchical carbon nanotubes with a thick microporous wall and inner channel as efficient scaffolds for lithium-sulfur batteries, Adv. Funct. Mater. 26 (10) (2016) 1571–1579.
[48] J. Cao, C. Chen, Q. Zhao, N. Zhang, Q. Lu, X. Wang, et al., A flexible nanostructured paper of a reduced graphene oxide-sulfur composite for high-performance lithium-sulfur batteries with unconventional configurations, Adv. Mater. 28 (43) (2016) 9629–9636.
[49] J.Y. Cheon, J.H. Kim, J.H. Kim, K.C. Goddeti, J.Y. Park, S.H. Joo, Intrinsic relationship between enhanced oxygen reduction reaction activity and nanoscale work function of doped carbons, J. Am. Chem. Soc. 136 (25) (2014) 8875–8878.
[50] Xue Liu, Jia-Qi Huang, Qiang Zhang, L. Mai, Nanostructured metal oxides and sulfides for lithium-sulfur batteries, Adv. Mater. 29 (20) (2017), https://doi.org/10.1002/adma.201601759.